Wiley Online Library
Early View publication on www.wileyonlinelibrary.com
(issue and page numbers not yet assigned;
citable using Digital Object Identifier – DOI)

J. Biophotonics 1–5 (2015) / **DOI** 10.1002/jbio.201500197

Journal of BIOPHOTONICS

LETTER

Integrated photoacoustic and diffuse optical tomography system for imaging of human finger joints *in vivo*

*Lei Xi**, [1, 2] *and Huabei Jiang**, [1, 2, 3]

[1] School of Physical Electronics, University of Electronic Science and Technology of China, Chengdu, Sichuan, China
[2] Center for Information in Biomedicine, University of Electronic Science and Technology of China
[3] Department of Biomedical Engineering, University of Florida, Gainesville, FL 32611, USA

Received 20 July 2015, revised 31 August 2015, accepted 10 September 2015
Published online 3 October 2015

Key words: photoacoustic imaging, diffuse optical tomography, quantitative reconstruction algorithm

In this study, we developed a dual-modality tomographic system that integrated photoacoustic imaging (PAI) and diffuse optical tomography (DOT) into a single platform for imaging human finger joints with fine structures and associated optical properties. In PAI, spherical focused transducers were utilized to collect acoustic signals, and the concept of virtual detector was applied in a conventional back-projection algorithm to improve the image quality. A finite-element based reconstruction algorithm was employed to quantitatively recover optical property distribution in the objects for DOT. The phantom results indicate that PAI has a maximum lateral resolution of 70 μm in resolving structures of targets. DOT was able to recover both optical absorption and reduced scattering coefficients of targets accurately. To validate the potential of this system in clinical diagnosis of joint diseases, the distal interphalangeal (DIP) joints of 4 healthy female volunteers were imaged. We successfully obtained high-resolution images of the phalanx and the surrounding soft tissue via PAI, and recovered both optical absorption and reduced scattering coefficients of phalanx using DOT. The *in vivo* results suggest that this dual-modality system has the potential for the early diagnosis of joint diseases such as osteoarthritis (OA) and rheumatoid arthritis (RA).

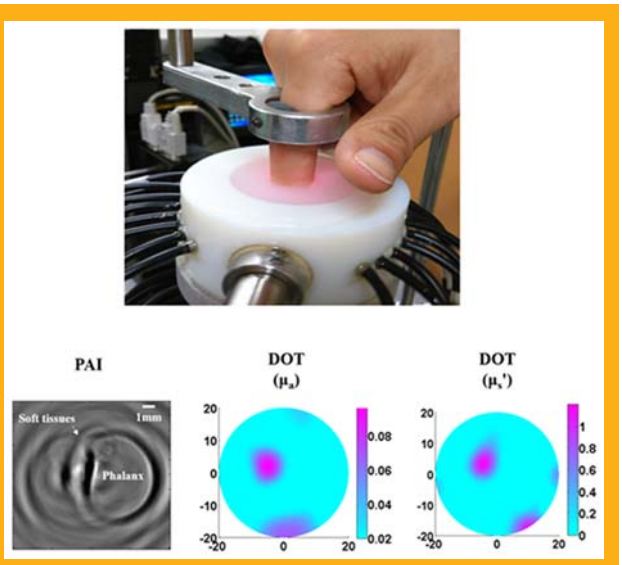

Integrated PAI/DOT imaging interface (top) and typical reconstruction of structures and associated optical properties of a female finger joint via PAI and DOT (bottom).

1. Introduction

Joint diseases such as osteoarthritis (OA) and rheumatoid arthritis (RA) are the leading cause of disability in the population over 50-year old. According to a clinical survey, millions of individuals over the world are suffering from OA [1]. Unfortunately, current clinical imaging techniques such as X-ray computed tomography (CT), magnetic resonance imaging (MRI) and ultrasound imaging (US) have in-

* Corresponding authors: e-mail: hjiang@bme.ufl.edu; xilei1985@uestc.edn.cn

herent limitations for routine diagnosis of early-stage arthritis [2–4]. For instance, X-ray has ionizing radiation with low sensitivity to soft tissues [2]. MRI suffers from low temporal resolution and high cost [3]. US is commonly used to evaluate the thickness of articular cavity in intermediate and advanced stages of arthritis [4].

With the advanced development of laser technologies, various optical imaging modalities such as photoacoustic imaging (PAI), diffuse optical tomography (DOT), fluorescence molecular tomography (FMT), optical coherence tomography (OCT) have been developed and widely used to diagnose joint diseases [5–10]. Among all of these imaging techniques, PAI, which utilizes the absorption of ultrashort light pulses by the tissue to induce wideband acoustic waves, owns greater depth penetration and spatial resolution [11, 12]. It has been successfully applied in the clinical detection of arthritis [5, 6]. However, it still has several inherent limitations: 1) the limited directivity of flat acoustic transducers which are commonly used in conventional circular-scanning-based PAI systems may lead to deterioration of resolution and deformation of reconstructed objects in off-center area/volume; 2) the axial resolution of circular/cylindrical scanning based PAI systems is determined by the aperture of the flat transducer which is commonly several millimeters; 3) PAI can only provide high quality images for the targets with certain sizes matching the response band of the transducer; 4) another major challenge for PAI is to recover optical scattering properties of tissue since it is only sensitive to optical absorption [13]. In this study, to overcome the first challenge, we utilized focused transducers instead of flat ones and modified the traditional back projection reconstruction algorithm with the concept of virtual detector proposed by Wang's group [14, 15]. In addition, by utilizing cylindrical scanning and three-dimensional (3D) virtual-detector-based reconstruction algorithm, we have successfully obtained 3D structures of human DIP joints with 240 μm axial resolution that offers us more accurate 2D images comparing with conventional scanning-based systems [16]. DOT has the potential to overcome some of the limitations associated with PAI, since it's able to fully recover different sized targets and quantitatively derive their optical absorption and scattering properties; however, the insufficient spatial resolution of DOT hinders its growth in both biomedical research and clinical applications [7, 8]. Following our previous study that integrated an array-based PAI and optical fiber based DOT for clinical detection of breast cancer [13], in this study, we further improved the performance of PAI and developed a compact system specifically designed for imaging human finger joints.

2. Methods

2.1 Integrated imaging system

Figure 1 presents the block diagram of our PAT/DOT imaging system where the illuminating light of DOT generated from a diode laser (M5-785-0080, Thorlabs) with a wavelength of 785 nm was delivered sequentially by an optical switch and 8 optical fiber bundles to source positions. For each excitation, diffused photons collected by another 8 fiber bundles and a cooled CCD (Princeton Instruments, Trenton NJ) was used for data collection. For PAI, the near-infrared (NIR) pulses generated from an OPO pulsed laser (Surelite I-20, Continuum, CA) with a duration of 6ns and a repetition rate of 20 Hz was split and coupled into four high energy optical fiber bundles positioned near ultrasonic transducers (Figure 2). The generated wide band acoustic signals were collected by two spherical transducers (V320-SU, Olympus, MA), which have the same aperture (19 mm in diameter) and focal length (25.4 mm). Two pre-amplifiers (5072PR, Olympus, MA) and a 12-bit dual channel data acquisition card (NI5124, National Instruments Corporation, TX) were used to amplify and record the acoustic signal.

The detailed schematic of the imaging interface is shown in Figure 2. The ring-shaped plastic holder had an internal radius of 25.4 mm equaling to the focal length of transducers. Two transducers were symmetrically positioned and manually adjusted in order to make sure that the focal points were overlapped with the center of the holder. Sixteen optical fiber bundles were uniformly distributed and co-axially positioned in source/detection positions inside the holder. During the phantom experiments, DOT was carried out first to avoid the interference with the excitation light of PAT. After the collection of the DOT data, the wavelength of the pulsed laser was tuned to 720 nm in the NIR window. This was done to obtain good penetration and PAI data was collected. In PAI experiments, the measured pulsed

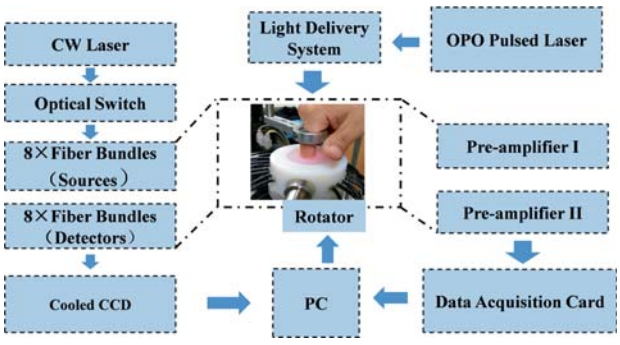

Figure 1 The block diagram of the hybrid PAI/DOT imaging system.

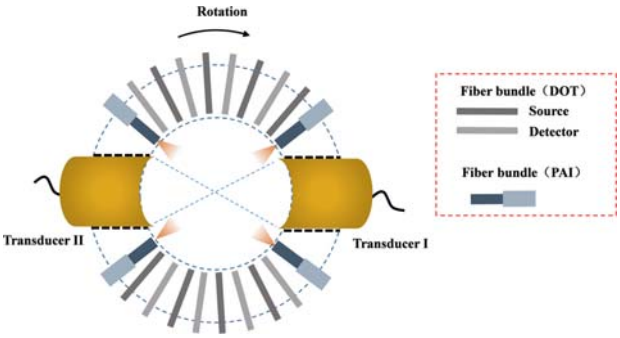

Figure 2 The schematic of the imaging interface.

energy per fiber bundle was 3.5 mJ. This leads to 2.8 mJ/cm^2 on the surface of the phantom, which was below the ANSI safety limit of 22 mJ/cm^2. The whole imaging interface was mounted on a rotator and took 6 seconds to scan 120 steps with a constant interval of 1.5° to cover a 360° receiving angle without any signal averaging. For three-dimensional data collection, the imaging interface was axially scanned 80 steps with an interval of 200 μm. The total experimental time was 490 seconds and time of 3D reconstruction was 5 minutes.

2.2 DOT reconstruction

The finite element based reconstruction algorithm was modified from our previous algorithms described in detail by Li and Jiang [17, 18]. Briefly, the algorithms use a regularized Newton's method to update an initial optical property distribution iteratively in order to minimize an object function composed of a weighted sum of the squared difference between computed and measured optical data at the medium surface. The computed optical data such as photon density is obtained by solving the photon diffusion equation with a finite element method. The core procedure in our reconstruction algorithms is to iteratively solve the following regularized matrix equation:

$$(\mathfrak{J}^T\mathfrak{J} + \lambda I)\,\Delta q = \mathfrak{J}^T(\Phi^{(m)} - \Phi^{(c)}) \qquad (1)$$

where Φ, I and λ represent the photon density, an identity matrix and a diagonal matrix.

$$\Delta q = (\Delta D_1, \Delta D_2, \ldots, \Delta D_N, \Delta\mu_{a,1}, \Delta\mu_{a,2}, \ldots, \Delta\mu_{a,N})^T$$

is used to update the optical property profiles, where N is the total number of nodes in the mesh and D is the diffusion coefficient. $\Phi^{(m)} = (\Phi_1^{(m)}, \Phi_2^{(m)}, \ldots, \Phi_M^{(m)})$ and $\Phi^{(c)} = (\Phi_1^{(c)}, \Phi_2^{(c)}, \ldots, \Phi_M^{(c)})$, where $\Phi_i^{(m)}$ and $\Phi_i^{(c)}$ are measured and calculated data for $i = 1, 2, \ldots, M$ boundary locations. $\mathfrak{J}$ is the Jacobian matrix that is formed by $\partial\Phi/\partial D$ and $\partial\Phi/\partial\mu_a$ at the boundary measurement sites. In DOT reconstruction, the goal is to update the optical absorption and diffusion coefficients or to reduce scattering coefficient through the iterative solution of Eq. (1) in order to minimize the weighted sum of the squared difference between computed vs measured data. In the code, a single mesh of 700 nodes were used, and the images were converged within 15 iterations in a PC with 1GB memory.

2.3 Phantom and pre-clinical experiments

Several phantoms were prepared to evaluate the performance of this system. The tissue-mimicking liquid was made by mixing Intralipid and ink, which served as the optical scattering and absorption of normal human tissues. The scattering and absorption properties of the cylindrical targets with sizes of 6 mm and 10 mm were simulated via the Intralipid and ink solutions too. Both background and target solutions, were solidified by Agar. In order to test the lateral resolution of PAI, carbon fibers with a size of 6 μm in diameter were embedded inside the background phantom. For all experiments, the imaging area were filled with tissue mimicking background solutions.

3. Results and discussion

Figure 3a shows the reconstructed photoacoustic image of a carbon fiber. We plotted the profile across the carbon fiber to measure its imaged size, which was 70 μm in order to determine the maximum lateral resolution of PAI. In addition, we found that the imaging quality out of the active imaging area with a radius of 5.5 mm descended quickly. Theoretically, the active imaging area depends on the effective focal zone of the focused transducer, which was measured to be 5.5 mm for the transducers used in this system. However this is not the fundamental restriction of our system. In different applications, we can choose transducers with various focal lengths or use variable-focus transducers developed by our group for a specific application. Figure 3b shows the DOT and PAI images of two targets, which have different sizes of 6 mm and 10 mm in diameter, and owns the same optical absorption coefficient and reduced optical scattering coefficient of 0.08 mm^{-1} and 1.2 mm^{-1}. Both targets were used to simulate the geometry and optical properties of joint phalanx. PAT and DOT could recover the targets, however, the imaged geometry of PAI is more accurate than that of DOT for both targets. We note that the geometry of the targets reconstructed by DOT are el-

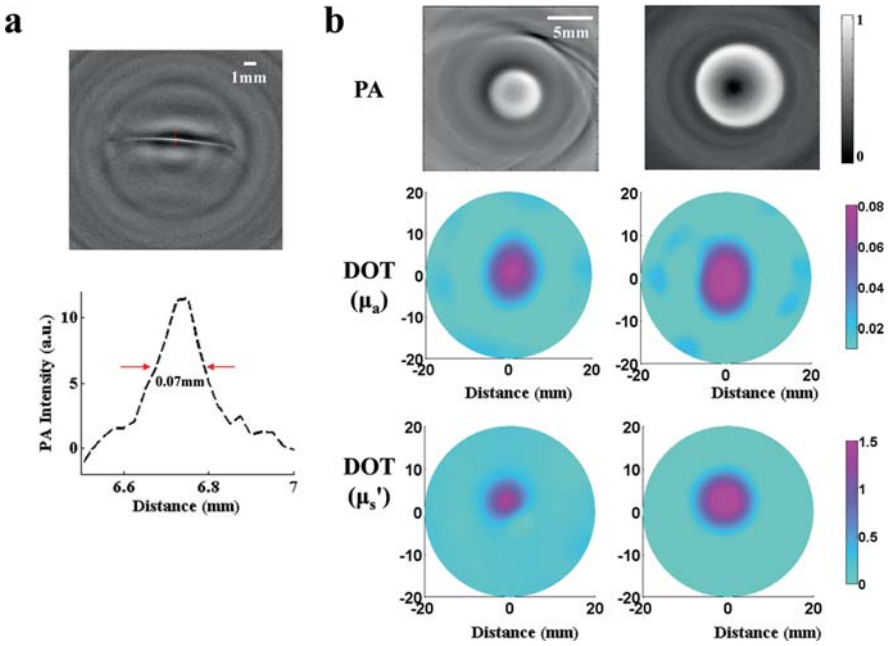

Figure 3 The results of phantom experiments. (**a**) The photoacoustic image of a carbon fiber embedded in a tissue mimicking phantom and the cross profile along the red dashed line in the image. (**b**) Photoacoustic and DOT images of finger phalanx mimicking targets.

lipsed. This is due to the limited view of data collection in DOT experiments. Besides compensated by PAI, we can further improve the image quality of DOT by employing more sources and detectors in the setup or rotating the imaging probe to obtain DOT data in a view of 360°. Quantitatively, in Figure 3b, both absorption and reduced scattering coefficients of the targets are accurately recovered by DOT. Interestingly in PAI, we found that partial information inside the 10 mm target were missed due to the loss of the low frequency signal given the limited frequency response of the transducers. However, DOT in this case provides both accurate recovery of the target in terms of its size, position and optical parameters. This finding agrees well with our previous studies and reveals the benefit of the dual modality strategy [13]. The phantom results validate the feasibility of this hybrid system in imaging of phalanx inside human finger joints *in vivo* in next section.

For clinical validations, we recruited 4 female volunteers and imaged the distal interphalangeal (DIP) joints of their middle fingers using PAI and DOT. A typical photoacoustic image is shown in Figure 4 where we can clearly identify the phalanx and soft tissues surrounding the phalanx. Furthermore, the optical absorption and reduced scattering coefficients of the phalanx are accurately recovered by DOT and agree well with the values (absorption: 0.07 ~ 0.11 mm^{-1}; scattering: 1.2 ~ 1.9 mm^{-1}) in the Refs. [19, 20]. From both phantom and *in vivo* experiments, we found that there were boundary noises in absorption images of DOT. This is caused by the strong optical absorption of transducer surfaces, which are coated with black material.

4. Conclusion

In sum, we developed a dual-modal photoacoustic and diffuse optical tomographic system and evaluated its performance via phantom and *in vivo* human experiments. This system takes full advantages of PAT and DOT to provide high resolution geometrical and function-associated information of phalanx inside human finger joints. Before we translate this system to the clinical stage in early diagnosis of ar-

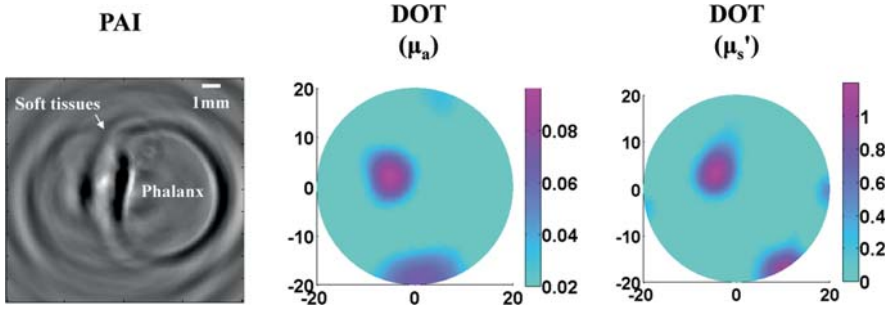

Figure 4 PAI and DOT images of a typical phalanx inside the middle finger of a female volunteer.

thritis patients in the future, we note that there are still several improvements that need to be undertaken. First, multispectral strategy should be employed by DOT to provide functional parameters such as oxygen saturation and concentrations of hemoglobin. Second, due to different sound velocities of tissues in finger joints, there are artifacts in the images recovered by current linear reconstruction algorithm. We are currently developing finite-element based quantitative reconstruction algorithm considering different sound velocities of tissues. Third, we could use the high-resolution geometrical information and optical absorption property provided by quantitative PAI to guide the reconstruction of DOT that will significantly improve the image quality of DOT [21]. In addition, we are aware that more sources and detectors as well as rotation of the imaging probe are required to reconstruct the joints more accurately via DOT. Finally, we could develop the three-dimensional (3D) PAI/DOT system by using multi-layer sources/detectors for DOT and axial scanning of the imaging interface for PAI.

Acknowledgements This work was sponsored by National Natural Science Foundation of China (81571722 and 61528401), startup grant (A03012023601011) from University of Electronic Science and Technology of China and in part by the J. Crayton Pruitt Family endowment fund.

References

[1] F. W. Roemer and A. Guermazi, Osteoarthritis and Cartilage **22**, 2003–2012 (2014).
[2] F. W. Roemer, M. D. Crema, S. Trattnig, and A. Guermazi, Radiology **260**(2), 332–354 (2011).
[3] J. A. Tyler, P. J. Watson, H. L. Koh, N. J. Herrod, M. Robson, and L. D. Hall, Acta Orthoped. Scand. Suppl. **266**, 130–138 (1995).
[4] S. L. Myers, K. Dines, D. A. Brandt, K. D. Brandt, and M. E. Albrecht, J Rheumatol. **22**(1), 109–116 (1995).
[5] Y. Sun, E. Sobel, and H. Jiang, J. Biomed. Opt. **14**(6), 064002-1–5 (2009).
[6] X. Wang, D. Chamberland, and D. Jamadar, Opt. Lett. **32**(20), 3002–3004 (2007).
[7] Z. Yuan, Q. Zhang, H. Jiang, E. Sobel, and H. Jiang, Proc. SPIE. **7174**, 71740K (2009).
[8] A. H. Hielscher, A. D. Klose, A. K. Scheel, B. Moa-Anderson, M. Backhaus, U. Netz, and J. Beuthan, Phys. Med. Biol. **49**(7), 1147–1163 (2004).
[9] P. van Es, S. K. Biswas, H. J. Bernelot Moens, W. Steenbergen, and S. Manohar, J. Biomed. Opt. **19**, 060501 (2014).
[10] A. Scheel, M. Backhaus, A. Klose, B. Moa-Anderson, U. Netz, K. Hermann, J. Beuthan, G. Muller, G. Burmester, and A. Hielscher, Ann Rheum Dis. **64**(2), 239–245 (2004).
[11] L. V. Wang and S. Hu, Science **335**, 1458–1462 (2012).
[12] P. Beard, Interface Focus., **1**, 602–631 (2011).
[13] L. Xi, X. Li, L. Yao, S. Grobmyer, and H. Jiang, Med. Phys. **39** (5), 2584–2594 (2012).
[14] L. Nie, Z. Guo, and L. V. Wang, J. Biomed. Opt. **16**, 076005-1–5 (2011).
[15] C. Li and L. V. Wang, Journal of Biomedical Optics **14**, 024047-1–3 (2009).
[16] L. Xi and H. Jiang, Appl. Phys. Lett. **107**, 063701 (2015).
[17] C. Li and H. Jiang, Opt. Express **12**(25), 6313–6318 (2004).
[18] H. Jiang, N. V. Iftimia, Y. Xu, J. A. Eggert, L. L. Fajardo, and K. L. Klove, Acad. Radiol. **9**(2), 186–194 (2002).
[19] A. Pifferi, A. Torricelli, P. Taroni, A. Bassi, E. Chikoidze, E. Giambattistelli, and R. Cubeddu, J. Biomed. Opt. **9**(3), 474–480 (2004).
[20] A. N. Bashkatov, E. A. Genina, V. I. Kochubey, and V. V. Tuchin, Optical Technologies in Biophysics and Medicine VII. **6163**, 616310 (2005).
[21] A. Q. Bauer, R. E. Nothdurft, T. N. Erpelding, L. V. Wang, and J. P. Culver, J. Biomed. Opt. **16**(9), 096016 (2011).